2009

Room Temperature Synthesis And Systematic Characterization Of Ultra-small Ceria Nanoparticles

Chetak Patel
University of Central Florida

University of Central Florida

Showcase of Text, Archives, Research & Scholarship

ROOM TEMPERATURE SYNTHESIS AND SYSTEMATIC

CHARACTERIZATION OF ULTRA-SMALL CERIA

NANOPARTICLES

by

CHETAK PATEL

Bachelor of Pharmaceutical Sciences, Nagpur University, 2005

A thesis submitted in partial fulfillment of the requirements
for the degree of Master of Science
in the Department of Chemistry
in the College of Sciences
at the University of Central Florida
Orlando, Florida

Fall Term 2009

ABSTRACT

Cerium oxide (ceria, CeO_2) is a rare earth oxide that has attracted wide-spread research interest because of its unique properties such as high mechanical strength, oxygen ion conductivity, oxygen storage capacity and autocatalytic property. In recent years, researchers have discovered that ceria nanoparticles (NPs) are capable of protecting cells from free radical induced damage. Interestingly, it was found that nanometer size (~ 5 nm) ceria can scavenge free radicals quite efficiently, thus acting as an anti-oxidant. This phenomenon has been explained based on the autocatalytic property of ceria NPs. Several methods have been developed for the synthesis of ceria NPs that include flame combustion, hydroxide co-precipitation, hydrothermal/solvothermal, microemulsion, sonochemical and microwave-assisted heating methods and sol-gel method. Ceria NPs synthesized by these methods are often highly aggregated. Furthermore, large scale synthesis of monodispersed CeO_2 NPs is quite challenging. Therefore it is desirable to synthesize ceria NPs in bulk quantity keeping its important properties intact, specifically free-radical scavenging property. The main goal of this study is therefore to synthesize ultra-small (< 5.0 nm), high quality monodispersed ceria NPs in large quantities.

In this thesis work, I present a couple of room temperature techniques, dilute sodium hydroxide (NaOH) assisted and ethylenediamine (EN) assisted for the synthesis of nearly mono-dispersed, ultra-small (< 5 nm) and water-dispersible ceria NPs. Morphology and particle size of the ceria NPs were investigated through high resolution transmission electron microscopy (HRTEM). The HRTEM analysis confirmed the formation of 3.0 ± 0.5 nm size and 2.5 ± 0.2 nm size highly-crystalline ceria NPs when synthesized using dilute NaOH and EN as solvents, respectively. The nanostructures were characterized by X-ray diffraction (XRD) studies to determine the crystal

structure and phase purity of the products. The samples were also thoroughly characterized by X-ray photoelectron spectroscopy (XPS) to determine the oxidation state of cerium ions. The presence of the +3 and +4 oxidation states in the samples was also confirmed from the XPS analysis. The co-existence of these two oxidation states is necessary for their applications as free radical scavenger. The autocatalytic behaviors of the ceria NPs were investigated through a hydrogen peroxide test and monitored by UV-visible transmission spectroscopy.

I would like to dedicate my thesis to my Father Mr. Sureshbhai Patel and my Mother Mrs.

Rasika S. Patel.

ACKNOWLEDGMENTS

Patel, Kaushal Singh, Saral Shah, Palak Patel, Sonal Patel and Balasubramanium Lingam, for all their love and affection. They stood by me in both good and hard times and made life easier for me at UCF.

Above all, I would like to thank my father Sureshbhai Patel and mother Rasikaben Patel, my sister Jaimini and brother Dr. Vikas for their limitless sacrifices for my happiness. I would like to give full credit to my family without whom this thesis would never have been realized.

TABLE OF CONTENT

LIST OF FIGURES

LIST OF TABLES

CHAPTER 1: INTRODUCTION

1.1 Nanotechnology: An Overview

The future of nanotechnology was predicted on December 29, 1959 by Nobel laureate physicist Richard Feynman in his classic lecture "There's Plenty of Room at the Bottom" delivered at the American Physical Society meeting at California Institute of Technology, USA. In his lecture, he mainly focused on the field of miniaturization and suggested that devices and materials could be fabricated at atomic specifications. Specifically, he said "The Principle of physics, as far as I can see, do not speak against the possibility of maneuvering things atom by atom."[1] In 1974 Norio Taniguchi, a professor of Tokyo Science University used the term "nanotechnology" in his article on ion-sputtered machining to represent extra high precision and ultra high dimensions. According to him "Nanotechnology mainly consists of the processing of separation, consolidation, and deformation of materials by one atom or one molecule."[2]

 Later in 1977 K Eric Drexler who was greatly inspired by Feynman's ideas originated "molecular nanotechnology" concept which involves the self assembly of molecules into an ordered and functional structure. In his book '***Engines of Creation'*** Drexler discussed the creation of larger objects from their atomic and molecular components; known as 'bottom-up approach'.[3]

In 1981 Gerd Binning and Heinrich Rohrer invented the scanning tunneling microscope (STM) at IBM laboratories in Zurich. This discovery led to the direct visualization of materials in nanoscale. The STM provided a unique opportunity to manipulate materials at atomic level and to record the resulting nanostructure. This was then followed by the invention of atomic force microscopy (AFM) in 1986, which again allowed scientists to image structures at atomic

scale. Another major breakthrough took place in 1985 with the discovery of new form of carbon called fullerenes [4] (buckyballs) by Harry Kroto, Robert Curl and Richard Smalley, who shared Nobel Prize in 1996 for this discovery. A fullerene is a single molecule of 60 carbon atoms arranged in shape of soccer ball, an example of bottom-up nanofabrication approach, all these developments enabled scientist to term nanotechnology as one of the most promising field of science of modern era.

1.2 Nanomaterial And Its Significance

Nanoscience deals with matter at nanoscale dimension, typically in the size range between 1 nm and 100 nm. Unique phenomena/novel properties (e.g. physical, chemical and biological) that are found in materials at the nanoscale enable nanotechnology and form a solid basis towards technological breakthrough. Interestingly, such properties are not observed at the atomic/molecular scale or at the bulk scale, thus making nanotechnology an emerging technology of the 21st century. A few example of nanoscale objects are summarized in Table 1 [3]. In order to enrich the nanoscience, it is extremely important to combine the experimental and theoretical findings. To achieve this, it is important to synthesize various nanostructures with control over their shape and size and subsequently characterize their physical and chemical properties. Proper analyses of these data along with the theoretical explanations are essential to understand the "nanoscale phenomena" of materials. This is essential for successful transfer of scientific knowledge to technology.[5]

Table 1. The sizes of nanoscale objects

Object	Diameter
Hydrogen atom	0.1 nm
Buckminsterfullerene (C60)	0.7 nm
6 Carbon atom aligned	1 nm
DNA	2 nm
Proteins	5-50 nm
Ribosome	25 nm
Virus	75-100 nm
Bacteria	1,000-10,000 nm
White blood cell	10,000 nm

Nanotechnology is based on interdisciplinary research in nanoscience that includes many disciplines such as physics, chemistry, materials science, biology and engineering. Research in this direction has been triggered by the availability of nanomaterial synthesis and fabrication techniques as well as sophisticated characterization tools, such as STM, AFM, HRTEM that in combination allow the investigation of nanomaterial size and nanoscale properties. The surface to volume ratio is much higher in NPs compared to their respective bulk materials. Therefore, surface atoms that are known to be in a different energetic state than the bulk atoms make significant contribution to the total free energy. These results in changes in the thermodynamic properties such as melting point [6] and solid-solid phase transition [7]. As the size of the material decreases, many physical phenomena solids are altered with great reductions in size. Changing

3

from macro to micro dimensions does not have larger impact on this effect, but it becomes a dominanting factor at the nanoscale.

Nanomaterial and nanocoatings are being used for bodies of aircraft and in aerospace components. Researchers have claimed that use of nanomaterial can increase the strength of aerospace materials by as much as 300 percent [8]. Nanocrystalline silicon nitride and silicon carbide have been used in spring ball bearings, and other automotive components [9]. For the fabrication and processing of nanomaterials and nanostructures, the following challenges must be met: (1) overcome the huge surface energy, a result of enormous surface area or large surface to volume ratio, (2) ensure all nanomaterials with desired size, uniform size distribution, morphology, crystallinity, chemical composition, and microstructure, that altogether result in desired physical properties and (3) prevent nanomaterials and nanostructures from coarsening through either Oswald ripening or agglomeration as time evolve. To combat these challenges, researchers are continuously developing synthesis protocols for nanomaterials and improving their surface coating technologies.

Since the past decade, a number of engineered NPs found wide applications in nanobiotechnology and nanomedicine [10]. In this direction, engineered NPs such as fluorescent semiconductor quantum dots, dye loaded polymeric NPs, magnetic NPs and gold NPs found various applications in nanobioimaging and sensing due to their unique optical and magnetic properties [10]. Another research direction that attracted a great deal of attention in recent years is fabrication of therapeutic nanoparticles. One such material which has found great interest in the past decade is the ceria NPs. Ceria NPs demonstrated strikingly different autocatalytic property compared to its bulk counterpart (larger crystals). Such catalytic property has attracted lots of

attention among many researchers worldwide for potential application in nanomedicine as a free radical scavenger [11-15].

1.3 Cerium Oxide (ceria)

1.3.1 Introduction to Cerium Oxide

Cerium is a rare earth element that belongs to the lanthanide group. Lanthanides are present in the earth's crust at 100 ppm, among all the lanthanides cerium is found in 24 ppm [16]. Several unique properties of cerium have been revealed by close examination of microcrystalline ceria structure, all properties differ significantly when compared with other rare earth materials [17].

All the other rare earth elements exists in trivalent states, but cerium atom can exist in fully oxidized (+4) state as well as fully reduced state (+3). In a redox reaction these two states interchange [17, 18]. As a result of alteration in the redox reaction, change in ceria crystal lattice (fluorite lattice structure) and the bond length is observed. The redox capacity of ceria is enhanced with loss of oxygen which creates oxygen vacancies or surface defects in the lattice structure[19].

Change in physical parameters like temperature, pH and oxygen partial pressure (pO_2), results in spontaneous change in the valence and defect structure of ceria [20]. At nanoscale, the characteristic properties of ceria are altered drastically compared to its bulk counterpart [21]. Presence of extremely high surface areas compared to bulk is important factor for the improved catalytic activity of the ceria NPs. In addition, the synthesis and thermodynamic conditions used to achieve ultra-small ceria NPs produce oxygen deficient ceria crystals. This type of oxygen deficiency in the crystal generates Ce^{3+} species in the CeO_2 lattice which causes the concurrent

presence of Ce^{3+} and Ce^{4+} valence state in the same crystallites introducing the anti-oxidant property in the material.

1.3.2 Applications of Cerium Oxide

Ceria is a useful material with applications as polishing agents [22], as an electrolyte for solid fuel cells [23], and also as a potential candidate for gate oxides in metal oxide semiconductor devices [23], as oxygen ion conductivity and oxygen storage capacity, autocatalytic properties and free radical scavenging property [14, 24-33]. Researchers have used ceria NPs in wide variety of applications. It has been used to coat metals which help to reduce oxidation [31] and also used as a coating material for catalytic converters thatenhanced the oxidation of carbon monoxide and hydrocarbons.

Recent studies have demonstrated that ceria NPs are capable of reducing free radical induced damage to rat brain cells which consisted of neurons, glia and microglia [11, 15, 34]. It is believed that the anti-oxidant property of ceria NPs increased longevity of neuron cells by reducing free radical damage commonly associated with aging and degenerative disorders of the central nervous system. It has also been demonstrated that ceria NPs particles are capable of protecting healthy cells from radiation damage in the treatment of cancer [15].

1.3.3 Synthesis of Ceria NPs

Several methods have been employed to synthesize ceria NPs including flame combustion method [35, 36], hydroxide co-precipitation of a precursor solution composed of cerium ammonium nitrate and zirconyl chloride followed by sonication [37], hydrothermal/solvothermal process [38, 39], microemulsion process [31, 40], sonochemical and microwave-assisted heating

6

methods [41], sol-gel method [42], base-catalysed aqueous precipitation method [13] etc. However, chemical synthesis of high-quality ceria NPs in large-scale remains a great challenge that demands developments of robust synthesis technique.

To date, the ceria NPs synthesized by above-mentioned methods are often highly aggregated and not useful even though there is almost 100% conversion of ceria chemical precusor to ceria NPs. Once aggregated particles are removed by centrifugation or filtration techniques, the yield of monodispersed ceria NP decreases that limits large scale synthesis. It is therefore important to develop a robust synthesis method that will address the above-mentioned limitations for producing water-dispersible, ultra-small (< 5 nm), crystalline ceria NPs that are highly monodispersed.

1.4 Research Objective

The main objective of my MS research was to develop robust synthesis techniques for producing ultra-small, water-dispersible, highly-monodispersed ceria NPs to meet the growing demand of high-quality ceria NPs.

CHAPTER 2: EXPERIMENTAL PROCEDURE

2.1 Materials

All the reagents were used as received. De-ionized (DI) nanopure water was used for all experiments. Reagent grade cerium nitrate (Ce $(NO_3)_3.6H_2O$), ethylenediamine and NaOH was purchased from Fisher Scientific. All the chemicals and solvents were of analytical grade and used without further purification.

2.2 Methods

Synthesis of NPs with controlled size and shape is highly challenging. The bottom up approach is highly accepted for the synthesis of ultra-small (<5 nm) NPs including ceria NPs. To control nucleation and growth processes, a highly controlled reaction environment is desirable. As discussed in Section 1.3.3, current ceria NP synthesis methods have certain drawbacks such as multi-step labor-extensive synthesis process, limited reproducibility and low yield of monodispersed ceria NPs. The choice of the technique is governed by factors such as size and shape selectivity, reproducibility, simplicity, large scale production, cost effectiveness etc. The purity and homogeneity of material are very important aspect from technological applications and needs to be taken into consideration while designing any synthetic method.

The present study involves the synthesis of ceria NPs at RT. The synthesis routes described herein are simple (one-pot synthesis), cost-effective and highly-reproducible. Products are free of large aggregates and the yield of monodispersed particles is quite high.

2.2.1 Sodium Hydroxide Assisted Synthesis of Ultra-Small Ceria NPs (S1)

Ceria NPs were synthesized by adding 0.434 g Ce $(NO_3)_3.6H_2O$ to a different concentration of basic solution (0.1 g, 2g, and 10g NaOH dissolved in 32 mL water) followed by 48 hrs magnetic stirring. The resulting white precipitate was collected and washed several times in water. Ceria NPs remained well dispersed in DI water for several days studied herein.

2.2.2 Ethylenediamine (EN) Assisted Synthesis of Ultra-small Ceria NPs (S2) at RT

The ultra-small ceria NPs were synthesized at RT by dissolving 0.234 g of $Ce(NO_3)_3.6H_2O$ in 32 mL EN with continuous stirring for 24 h upon which the solution turned light yellow [12]. The particles were recovered by centrifugation followed by washing in water. The particles were re-dispersed in DI water to obtain a faint yellow solution.

2.2.3 Solvothermal Synthesis of Ceria NPs (S3) Using EN at 180 ^{o}C

A Teflon-lined stainless steel cylindrical closed chamber with 40 mL capacity was used for the synthesis. Cerium nitrate salt was used as cerium precursor and EN as the base. The Teflon-lined chamber was filled up to 80% of its volume with EN and 0.234 g of cerium nitrate was added to the solution After 15 minutes of stirring, the closed steel chamber was placed inside a preheated oven for 8 hrs at 180°C [12]. The chamber was then allowed to cool down to RT. The resulting precipitate was filtered and washed several times with water.

2.2.4. Solvothermal Synthesis of Ceria NPs (S4) Using EN and water as solvent at 180 ^{o}C

The Teflon-lined chamber was filled with 80 % of its volume with equal ratio of EN and water (EN-W) and 0.234 g of cerium nitrate was added to the solution. After 15 minutes of stirring, the closed chamber was placed inside a preheated oven for 8 hrs at 180°C. The chamber was then allowed to cool down to RT. The resulting precipitate was filtered and washed several times with water [12].

2.3 Characterization Techniques

The physical and chemical properties of the ceria NPs were investigated by using various materials characterization techniques. XRD was used to determine the crystal structure and phase of products. Morphology of the nanostructure was studied from transmission electron microscopy (TEM). The high resolution transmission electron microscopy (HRTEM) was used to study the crystal structure of individual nanostructures. Optical absorption spectroscopy was used to study optical properties of the nanostructures. The chemical composition of the nanostructure was determined with X-ray photoelectron spectroscopy.

2.3.1 X-Ray Diffraction

XRD patterns were recorded on Rikagu D/MAX instrument with $CuK\alpha_1$ radiation with a scan rate of 0.25 degree min^{-1}.

2.3.2 X-Ray Photoelectron Spectroscopy

XPS spectra were obtained using a Physical electronic 5400 ESCA spectrometer with a base pressure of 10^9 Torr and $MgK\alpha$ X-ray radiation at a power of 200 W.

2.3.3 Transmission Electron Microscopy

TEM images were obtained using FEI TECNAI F-30 microscope operating at 300kV. The samples were prepared by placing a drop of solution containing ceria NPs on a thin carbon film coated copper 400 mesh grid.

2.3.4 Dynamic Light Scattering (DLS)

DLS experiments were performed on a PDDLS/Cool Batch 40T; PD2000 DDLS Measurements were taken by analysis the solution of ceria NPs in distilled water.

2.3.5 UV-Visible Spectroscopy

UV-Visible studies were performed on Varian Cary 300 Bio UV/Vis spectrometer.

CHAPTER 3: RESULTS AND DISCUSSION

3.1 Sodium Hydroxide Assisted Synthesis of Ultra-Small Ceria NPs

3.1.1 XRD Analysis

XRD pattern of the dried sample shown in Figure 1 confirmed the formation of phase pure CeO_2 with cubic phase (fluorite structure, JCPDS 34-0394, space group *Fm-3m*) having lattice constants of 5.414(3), 5.436(3), and 5.405(3) Å, respectively. The broadening of the diffraction pattern could be ascribed to the formation of ceria NPs. Within the limit of the XRD sensitivity, formation of any other phase such as hydroxide phase [$Ce(OH)_3$] could not be detected.
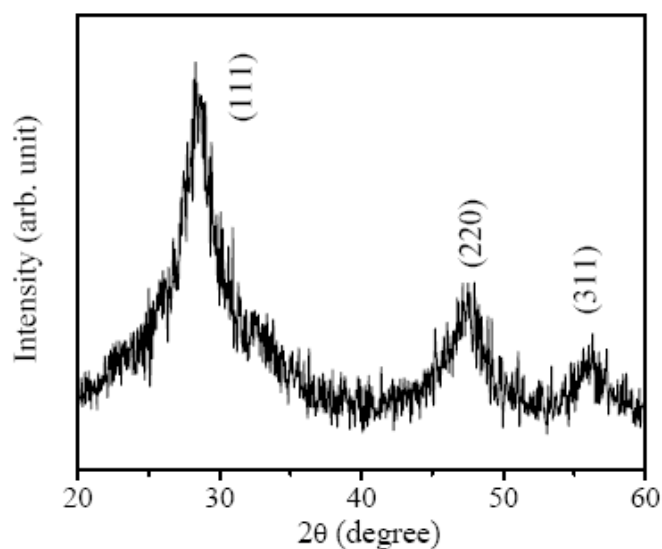
Figure 1 XRD pattern of the ceria NPs

3.1.2 TEM and DLS Analysis

The High Resolution TEM (HRTEM) study on ceria NPs was done to investigate the morphology and particle size of the particles. HRTEM image shown in Figure 2a clearly shows the formation of single crystalline ceria NPs at RT. It reveals the formation of nearly mono-dispersed ceria NPs with particle size 3.0 ± 0.5 nm. Image in the inset of Figure 2a shows the HRTEM image of a single ceria NP. Figure 2b represents the selected area electron diffraction (SAED) pattern recorded on a bunch of ceria NPs. The various crystalline plane of ceria NPs were indexed as the appearance of bright white ring on the SAED pattern. The results are in good agreement with the XRD pattern.

It was observed that the use of high concentration of NaOH triggered rapid and uncontrolled precipitation producing undefined aggregated ceria structures. Figure 3 reveals the formation of aggregated ceria structure with high concentration of NaOH. The particle size distribution and aqueous solubility was also characterized using DLS technique. The DLS data (Fig.4) also indicated the formation of nearly monodispersed particles with particle size 6.3 ± 1.0 nm. The appearance of the higher particle size in DLS as compared to the TEM is expected as the DLS provides the hydro-dynamic size of the particle in a solution.
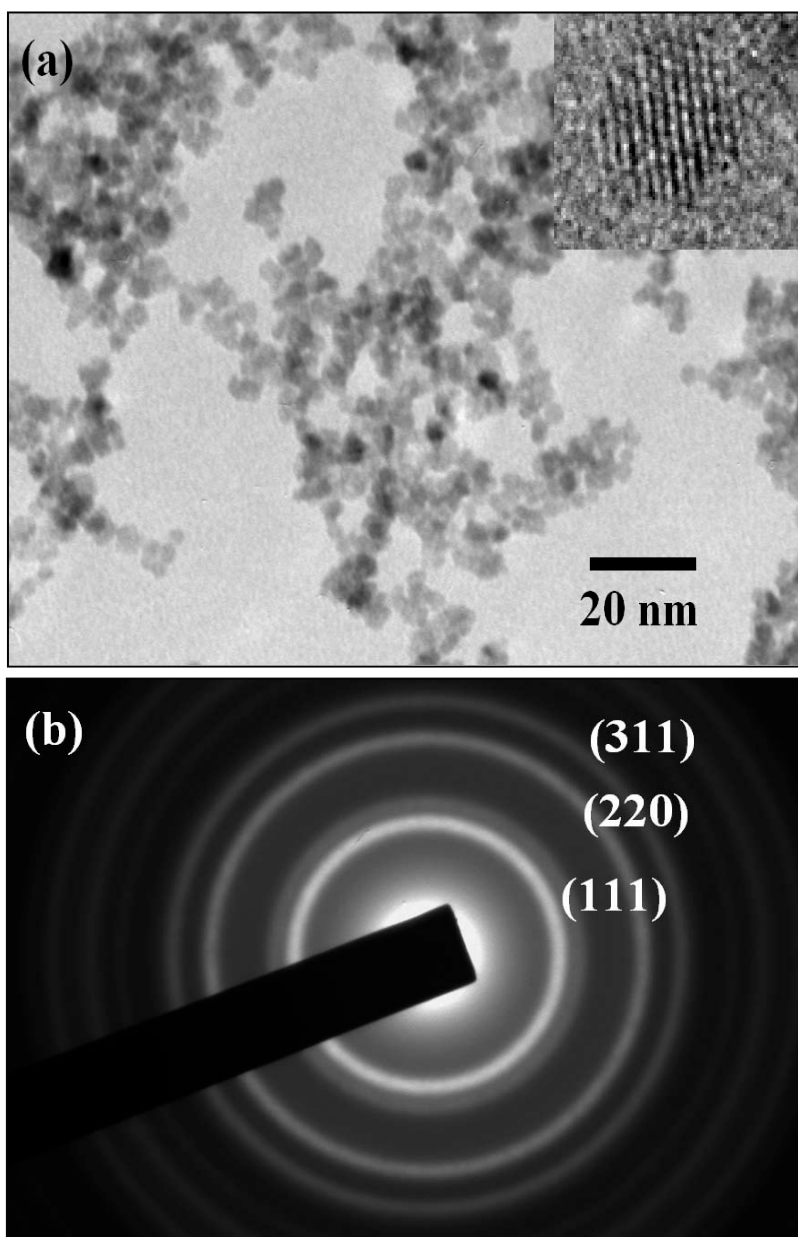
Figure 2 (a) TEM image shows the formation of mono-dispersed ceria NPs. The image in the inset depicted the high resolution TEM image of an individual NP. (b) SAED pattern of the NPs indicating the formation of crystalline ceria NPs
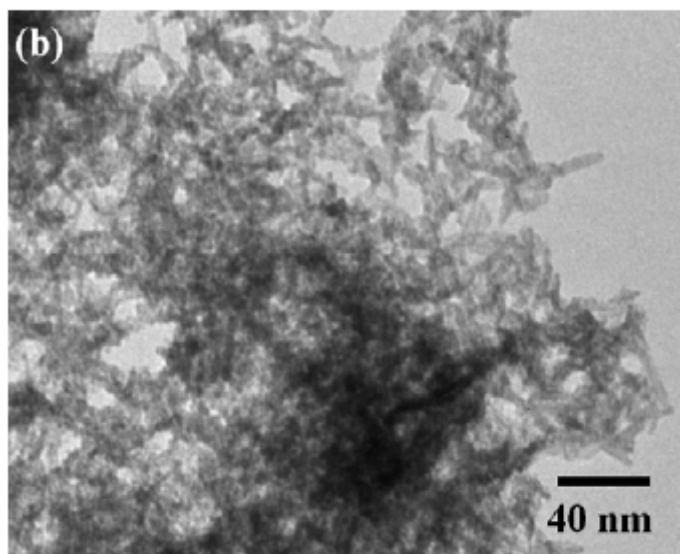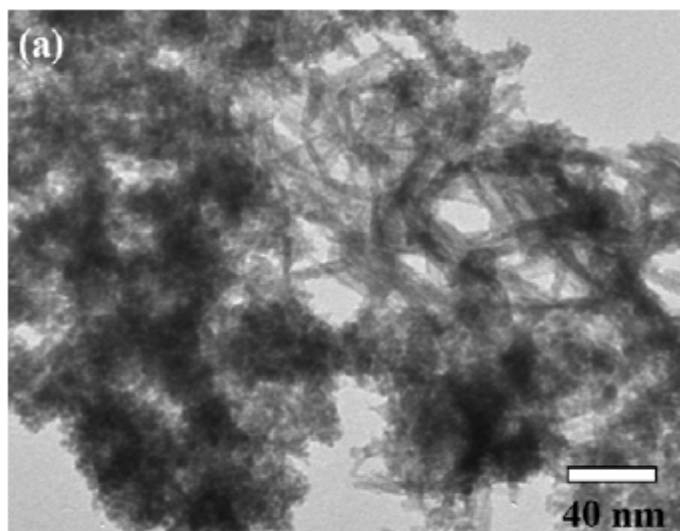
Figure 3 TEM image of the ceria precipitate obtained with: (a) 2 g and (b) 10 g NaOH
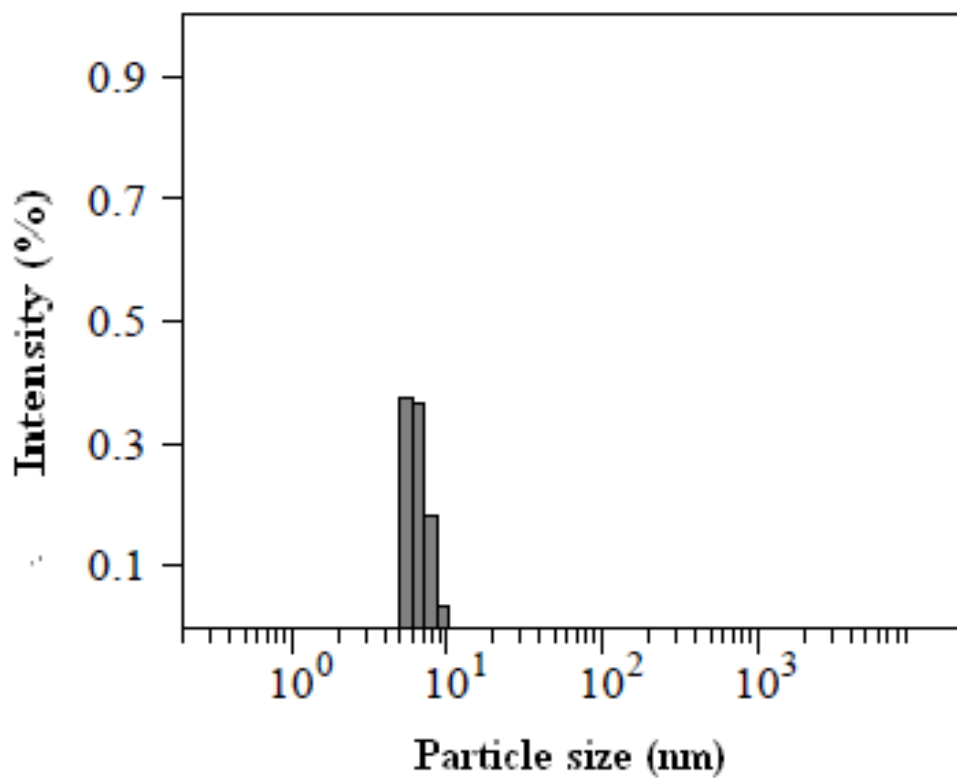
Figure 4 DLS Plot for the ceria NPs synthesized using low concentration of NaOH. It shows formation of nearly mono-dispersed ceria NPs

3.1.3 XPS Analysis

In order to determine the chemical composition and the valence state of the elementary components in the products we have carried out the XPS studies. It could be mentioned here that the XPS technology is not 100 % reliable technique to draw elementary compositions. But, a comparative study of more than one sample could indicate the elementary composition and environment of the constituent elements in the crystal lattice. Figure 5a shows the detailed XPS spectrum of the samples demonstrating the presence of Ce and O as the elementary components. It is well known that the valence state of the cerium is important in determining the properties and applicability of the ceria NPs. The high resolution XPS spectral analysis therefore provides details of the valence state of cerium in the region of 880-925 eV.

The XPS spectrum (Figure 5b) shows the presence of a mixed valence state (Ce^{3+} and Ce^{4+}) for the synthesized ceria NPs. The appearance of the Ce^{3+} valence state in the CeO_2 crystal lattice indicated the presence of oxygen vacancy centers in the ceria crystal lattice. Due to the oxygen vacancy, the coordination number of Ce^{4+} to O^{2-} reduces from eight to seven and introduces Ce^{3+} ions into the crystal lattice. Furthermore, the high resolution oxygen peak in the XPS spectra (Fig. 6a) reveals the presence of a solder peak at ~ 532 eV, which corresponds to the OH groups. Percentage of Ce^{3+} was calculated semi-quantitatively as 57.1 % using equation 1.

The presence of cerium hydroxide phase in the nanocrystals however, was not evident from the cumulative data analysis from XRD, HRTEM and SAED patterns. The presence of hydroxyl groups as evident from XPS must have originated from surface attached hydroxyl groups. NaOH played a critical role as a catalyst for transforming cerium salt to ceria and hydroxide ions served as a capping agent to prevent further grain growth.
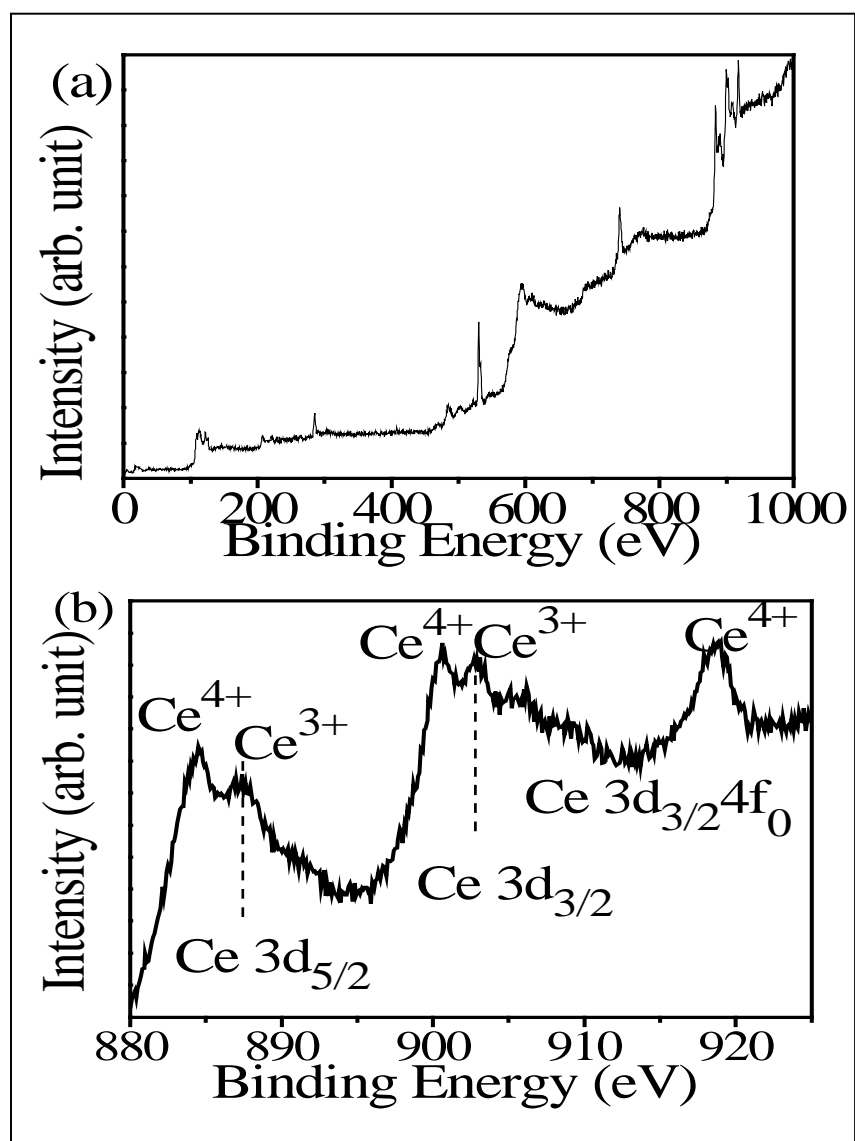
Figure 5 XPS spectra of the ceria NPs: (a) survey scan and (b) high-resolution scan showing the valence states for Ce in the ceria NPs
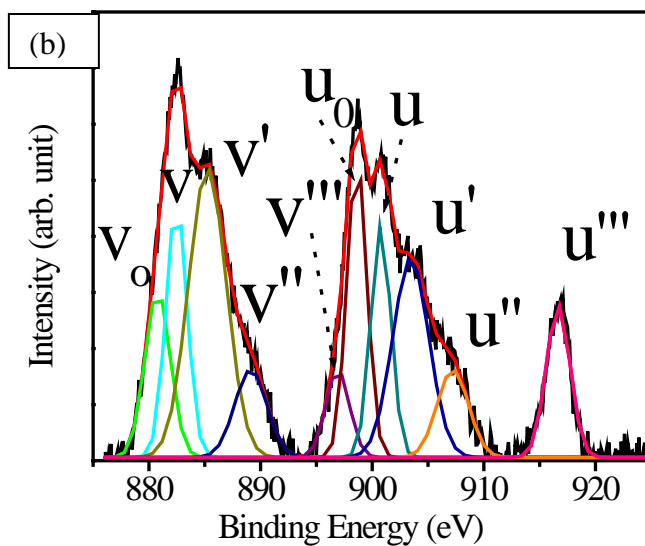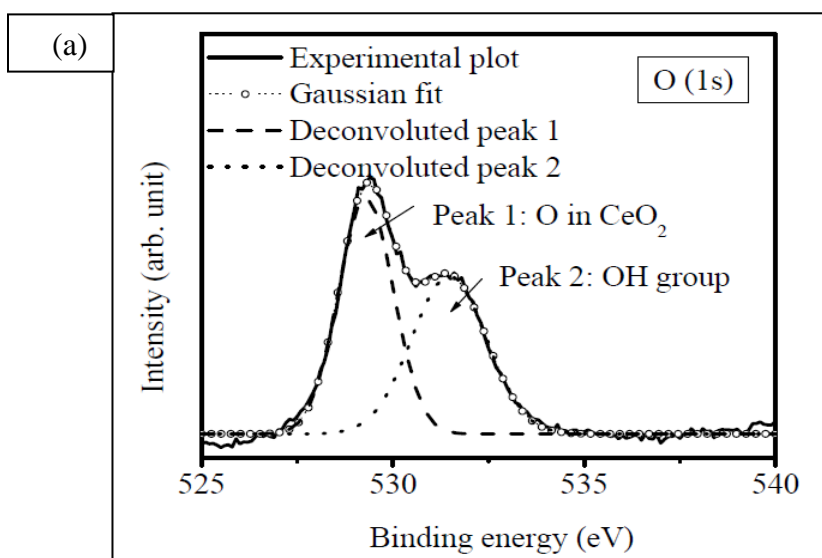
Figure 6 (a) High resolution XPS spectra showing the oxygen 1s peak recorded on the ceria NPs. The deconvoluted plot shows two peaks –one due to the oxygen in ceria and other attributed to the OH bond in NPs. (b) high-resolution plot along with the corresponding Gaussian fitting plot showing different valence states for Ce. In the figure, v_o, v', u_o, and u' peaks are attributed to Ce^{3+}; while v, v'', v''', u, u'', and u''' are the characteristic peaks of Ce^{4+}.

3.1.4 Autocatalytic Study

To demonstrate the auto-catalytic property of the ceria NPs, we carried out a UV–visible spectroscopic study in absence and presence of hydrogen peroxide (Figure 7a). The ceria NP solution in DI water was transparent and colorless as depicted in the digital images in the Figure 7b. First, the transmittance spectra of the water-dispersed ceria NPs were recorded. In the next step, 10 µl H_2O_2 was added to the above solution, stirred for 1 min and the transmission spectrum was measured again.

The transmission spectrum exhibited a large red shift when compared to the spectrum of ceria NP without H_2O_2. This is further substantiated by the drastic color change of the solution from clear to dark reddish-brown upon addition of H_2O_2. This red-shift in the transmittance spectrum is due to a change in the oxidation state from Ce^{3+} to Ce^{4+}.

The experimental solution was then kept in the dark and UV–visible spectra were recorded for the next 10 consecutive days. A gradual blue shift in the spectra was observed over time. This gradual blue shift reflects the regeneration of the Ce^{3+} oxidation state in the ceria NPs. At the end of the 10 days, the color of the solution faded away and became yellow. When an additional hydrogen peroxide dose was administered to the solution on day 10, the UV–visible spectrum again shifted to lower energy and subsequently the color of the solution again turned reddish-brown. With time, a gradual blue shift to the lower wavelength was observed, as seen previously.
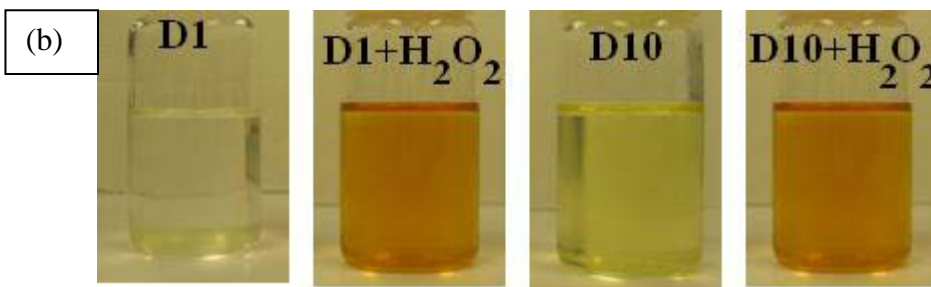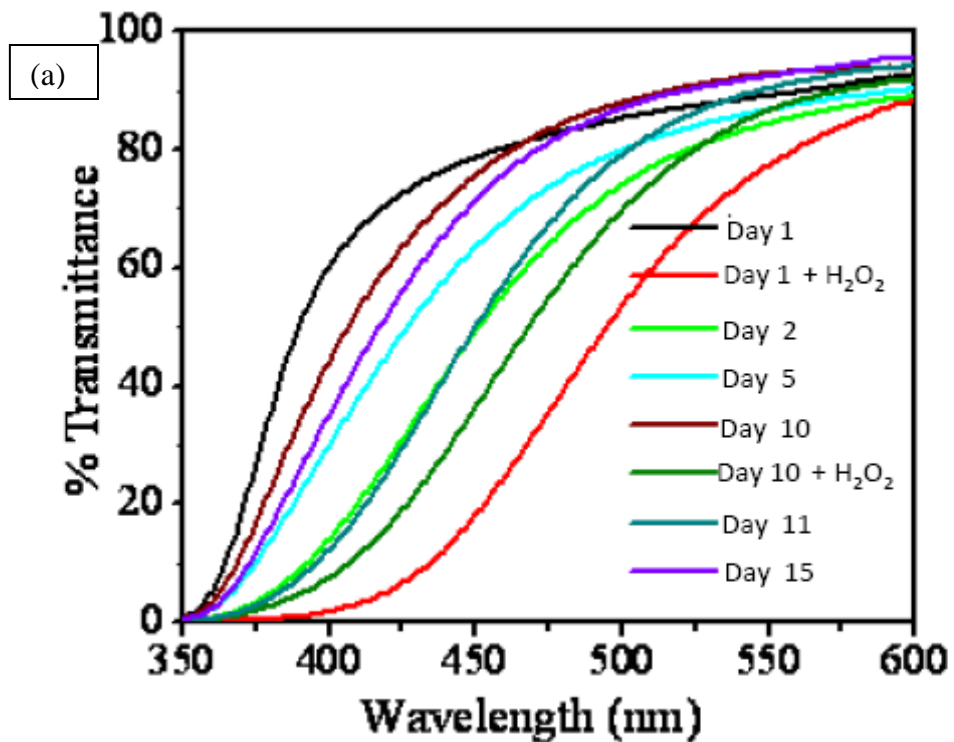
Figure 7 (a) UV-visible transmittance plots showing the autocatalytic behavior of the ceria NPs. (b) Digital images of the aqueous solution of the ceria NPs in absence and presence of H2O2 reflecting the valence state change are depicted in the inset.

The antioxidant property of the ceria NPs is controlled by the oxygen vacancy level in the nanocrystals. It has been proposed that the antioxidant property of ceria NPs are due to the presence of mixed valence states (Ce^{3+} and Ce^{4+}) on the NPs' surface. During the catalytic process, owing to oxidation Ce^{3+} ions are converted to Ce^{4+}. The system is regenerated via a series of surface chemical reactions between ions in solution and the Ce^{4+} ions on the NPs surface, which on subsequent reduction are converted back to Ce^{3+}. The complete process is depicted in the following reactions.

$$H_2O_2 \rightarrow 2[OH\cdot] \qquad (1)$$

$$Ce_2O_3 + 2[OH\cdot] \longrightarrow 2CeO_2 + H_2O \qquad (2)$$

$$2CeO_2 + H^+(aq) \rightarrow Ce_2O_3 + \frac{1}{2}O_2 \qquad (3)$$
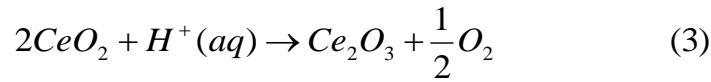
3.1.5 Growth Mechanism of the Ceria NPs

Based on our experimental findings, we propose the formation mechanism of ultra-small ceria NPs as follows. The controlled conversion of solvated cerium ions to ceria NP is mediated by the mild basic environment. Basic reaction condition instantaneously converts cerium hydroxide to ceria nuclei. The mild reaction condition is crucial for promoting controlled nucleation. During the growth process, hydroxide ions are populated to the surface bound cations, providing a unique capping environment. Such environment restricts grain growth by preventing further diffusion of the constituent

atoms. The present of large number of surface hydroxyl groups is responsible for superior aqueous dispersibility of ceria NPs. For biomedical applications, it is highly desirable to obtain water-dispersible high-quality ceria NPs in their native form. We have tested the state of NP dispersibility in phosphate buffer saline at physiological pH (pH 7.4) and found that particles remain well dispersed.

3.2 EN Assisted Synthesis of Ultra-Small Ceria NPs: Investigation On The Role of EN As capping agent

Water-dispersed particles were used to investigate the UV-visible and auto-catalytic activity of ceria NPs. The samples were characterized by suing XRD, XPS techniques to investigate their structural and chemical properties. The precipitate was recovered by centrifugation and it was washed several times with distilled water. The particles recovered after washing was used for further characterization. Approximately 100 % conversion was obtained in all the three samples synthesized in EN at RT, in EN at 180 ^{o}C and in EN-W at 180 ^{o}C. The crystalline phase of the products was identified by analyzing the XRD patterns recorded on the powder samples. Proper indexing of the XRD peaks (Figure 8) reveals the formation of cubic phase CeO_2 (JCPDS card number # 34-0394). The possibility of any other crystalline impurity in the ceria NP sample could be ruled out within the limit of sensitivity of XRD technique as no additional XRD peaks were found. Broadening of the diffraction patterns indicated the formation of ceria nanocrystals. Thus, XRD patterns indicated formation of smallest particle at RT and largest particle at the solvothermal condition in EN-W solvent.

23
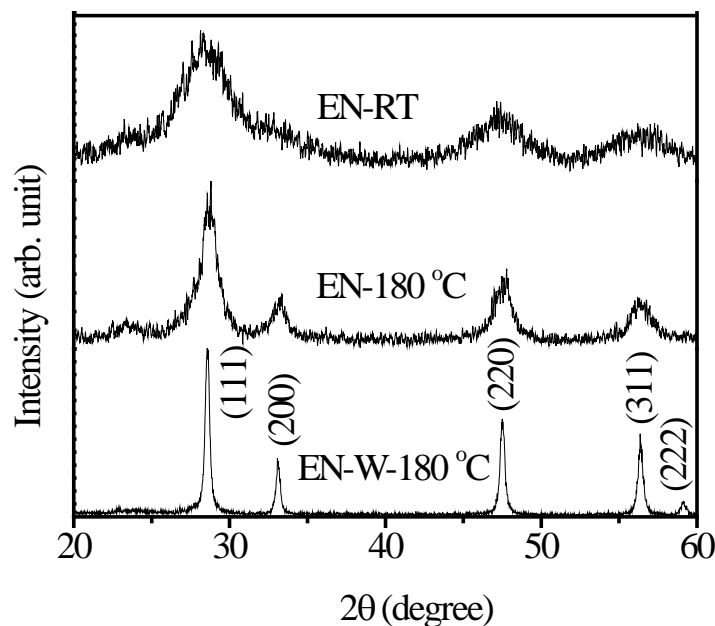
Figure 8 XRD patterns of the ceria NPs

Although the XRD studies reveal the formation of small ceria crystallites, however it is hard to predict whether the product is a polycrystalline precipitate or ultra fine individual nanocrystals. In order to elucidate the confusion about the morphology, the sample was further characterized by using HRTEM. Figure 9a depicts one representative HRTEM image revealing the formation of nearly mono-dispersed, ultra-fine ceria nanocrystals. The image clearly shows the formation of single crystalline particles with particle size 2.5 ± 0.2 nm. Formation of the cubic ceria nanocrystals is further confirmed by the SAED pattern shown in Figure 9b. The bright white rings in the SAED pattern are indexed to different crystalline planes of cubic ceria. The results are in good agreement with the XRD pattern. Thus the XRD and HRTEM studies indicated that

24

ultra-small ceria NPs could be synthesized using EN. Thus, it can be concluded that EN serves as a capping agent during the growth of ceria crystals. To further study the role of EN as a capping agent for the growth of ceria NPs, solvothermal syntheses were also carried out. XRD pattern indicates the formation of relatively larger particles at 180 ^{o}C. Figure 10a shows the HRTEM image of the ceria NPs formed in EN at 180 ^{o}C. The particle size was measured as 8.0 ± 1.5 nm. Higher temperature caused diffusion of more constituent elements inside the capping sphere, which is responsible for the particle size growth.

With the use of EN-W as solvent at 180 ^{o}C, poly dispersed particles were seen with size varying from 8-80 nm as shown in TEM image (Figure 10b). It could also be observed from the TEM image that the particles possessed a well defined cubic shape when water was introduced. The image in the inset of Figure 10b shows the HRTEM image of one such ceria cube.

Introduction of water reduced the capping ability of the EN, producing poly-dispersed particles. This proves that EN served as a capping agent during the growth of ceria NPs. The ceria NPs produced with EN at different conditions were dispersed in water under ultrasonic treatment. It was observed that only the particles obtained at RT were water soluble. Thus, with a view to test the dispersibility of the ultra-small ceria NPs in solution and determine the particle size in solution, DLS study was performed on Ceria NPs synthesized at RT, which shows formation of mono-dispersed ceria NPs (Figure 11) with hydrodynamic diameter 4.8 nm.
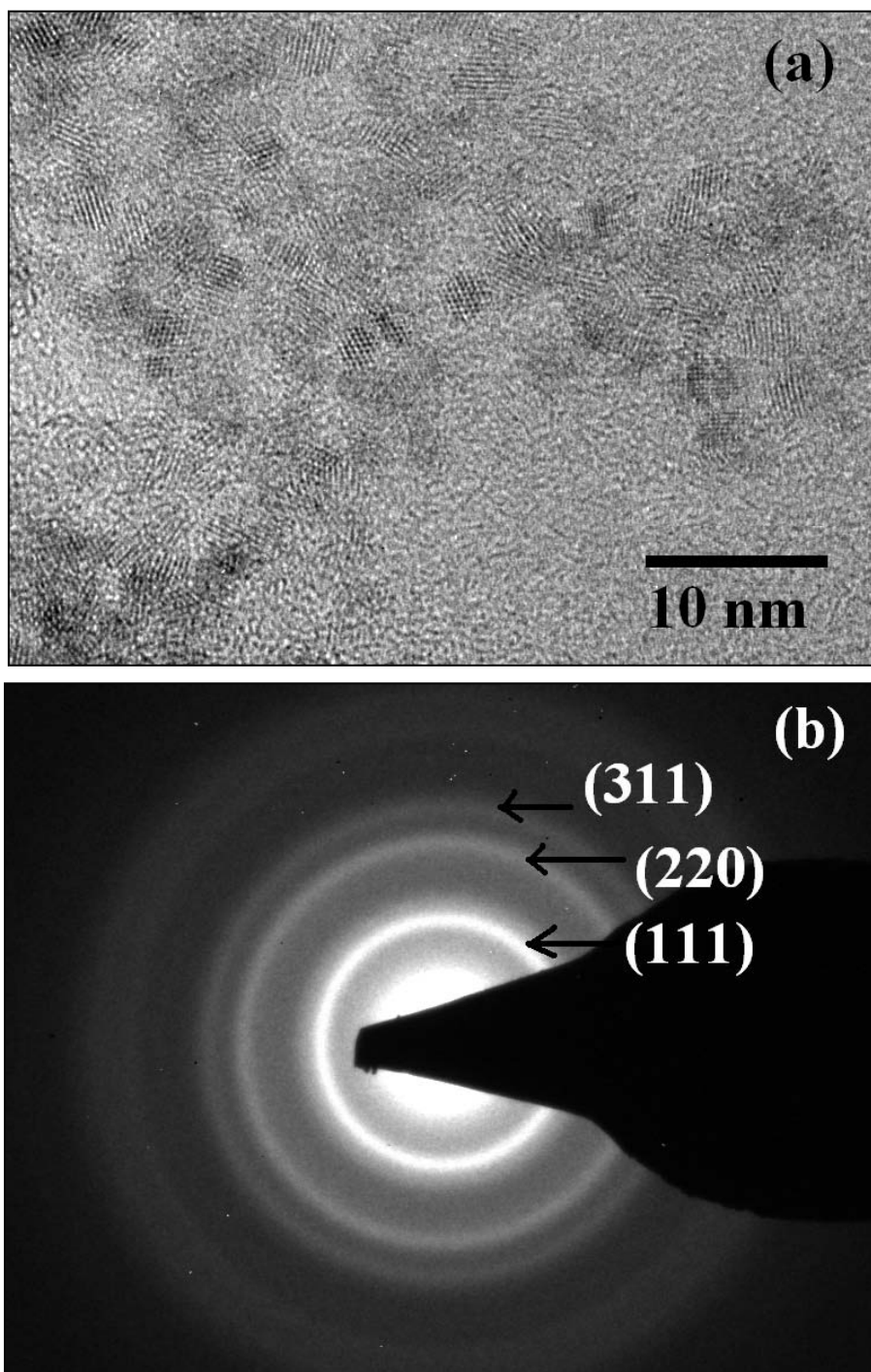
Figure 9 (a) HRTEM image shows the formation of mono-dispersed ceria ultra-small ceria NPs. (b) SAED pattern of the NPs indicating the formation of crystalline ceria NPs
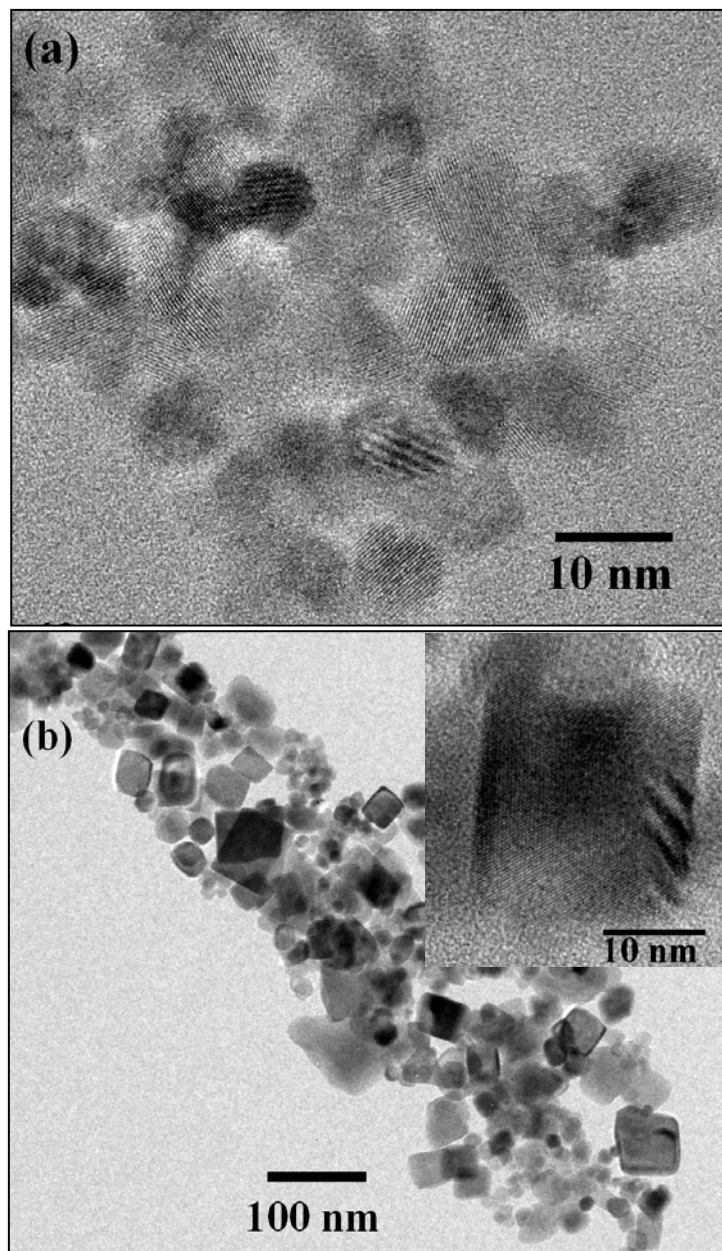
Figure 10 (a) HRTEM image of ~ 8 nm ceria NPs synthesized in EN at 180 ºC and (b)

TEM image of the poly-dispersed ceria NPs synthesized in EN-W at 180 ºC. The image

in the inset of part (b) shows the HRTEM of one ceria nano-cube.
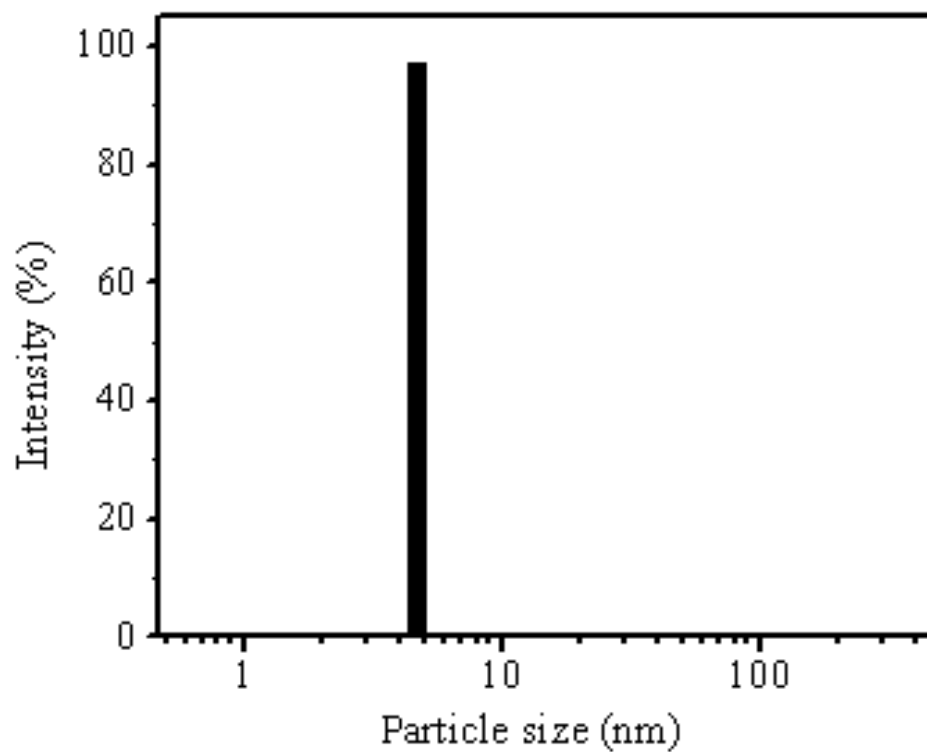
Figure 11 DLS plot showing the formation of mono-disperse ceria NPs at RT with hydrodynamic diameter 4.8 nm

Since the particles were synthesized in organic EN at RT with no further post heat treatment, there are possibilities that the EN could form a chelating complex with the cerium ions or the organic amine molecule could have remained attached to the NPs as surface adsorbed molecules. The XRD pattern shown in Figure 8 however, ruled out the possibility of any chelating complex formation between EN and Ce ions. Therefore IR studies were performed to test the presence of possible surface adsorbed EN molecules on the ceria NPs. Figure 12 shows the IR spectrum of the powder sample which was compared to that of pure EN. Absence of the sharp peaks in the 2700-3400 cm^{-1} region of the IR spectrum for ceria samples indicates the absence of EN in the sample. The broad hump could be attributed to hydroxyl groups.
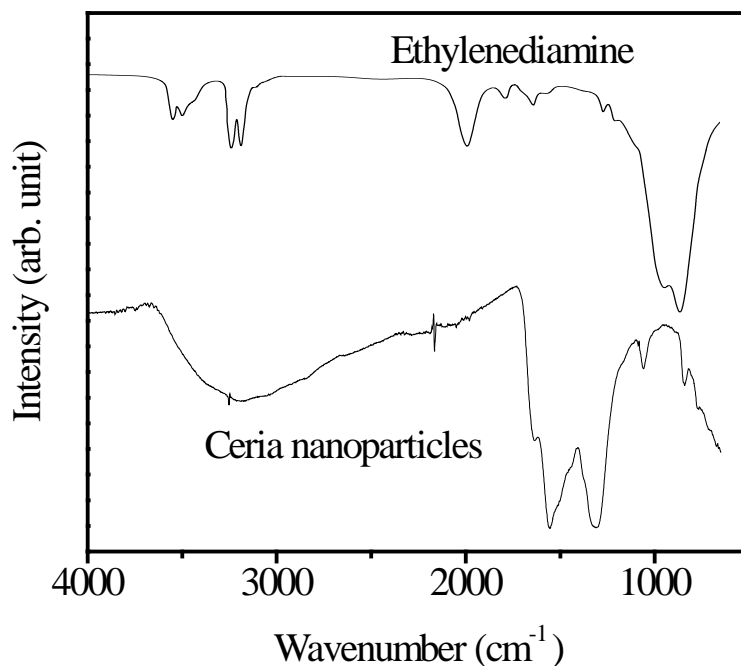
Figure 12 IR spectrum of the ceria NPs along with the IR spectrum of the pure ethylenediamine for comparative study

In recent years, superior antioxidant property of ceria NPs is attributed to their mixed valence state (Ce^{3+} and Ce^{4+}). It is highly desirable to fabricate ceria NPs where both the valence states co-exist. To confirm this we have carried out thorough XPS studies. Figure 13a demonstrates the survey XPS spectrum of the samples exhibiting the presence of Ce and O as the elementary components. The area of interest being the valence state of Ce, the high resolution XPS spectra were recorded in the region of 880-925 eV for all the samples. These high-resolution XPS spectra were deconvoluted to distinguish the Ce^{4+} and Ce^{3+} ionic states. All these spectra along with their Gaussian fits were displayed in Figures 13b-d. Indexing of the XPS spectrum reveals the presence of a mixed valence state (Ce^{3+} and Ce^{4+}). The peak positions and corresponding indexing were summarized for all the three samples in Table 2. In the figure, v_o, v', u_o, and u' peaks are attributed to Ce^{3+}; while v, v'', v''', u, u'', and u''' are the characteristic peaks of Ce^{4+}. The spectra show that the XPS peaks corresponding to Ce^{3+} valence state are relatively stronger at the RT synthesized samples. Whereas, the samples synthesized solvothermally in EN-W did not have any Ce^{3+} valence state. This shows that ceria NPs with engineered valence state could be synthesized using EN assisted chemical synthesis routes. Percentages of the Ce^{3+} and Ce^{4+} valence states could be semi-quantitatively analyzed by using the integrated peak area of the respective states using the following equation.[37]

$$[Ce^{3+}]\% = \frac{A_{v_o} + A_{v'} + A_{u_o} + A_{u'}}{A_v + A_{v''} + A_{v'''} + A_u + A_{u''} + A_{u'''}} \times 100\% \qquad (1)$$

where A_i, is the area of the "i" peak. The concentration of Ce^{3+} was calculated as 48.84 and 36.99 % for the ceria NPs synthesized with pure En at RT and 180 ^{o}C respectively. Thus the results indicated that the mixed valence state of the ceria NPs could be tailored by varying the synthesis temperature. The presence of Ce^{3+} ions in the ceria nanocrystal lattice is attributed to the oxygen

vacancies in the nanocrystals. The extent of the oxygen vacancy could be tailored in the nanocrystals by manipulating the synthesis conditions. Therefore our studies indicated that the present RT synthesis technique is robust and capable of producing valence state engineered ultra-small ceria NPs. Since the IR spectrum of the ceria NPs indicated the presence of hydroxyl groups, it is interesting to investigate the oxygen peak in the XPS. Figure 13e shows the high resolution XPS spectrum in the region 520-540 cm^{-1} showing the details of O1s peak. The peak clearly shows the presence of a shoulder peak corresponding to the hydroxyl groups. This result is in agreement with the IR spectra, confirming the presence of surface hydroxyl groups. Stable colloidal dispersion of these particles in water is perhaps due to these surface hydroxyl groups.

(a)

Ce 3d3

Ce 3d5

O1s

C 1s

Ce 4d5

Binding Energy (eV)

(b)

— Experimental plot
- - - Gaussian Fit plots

v'

v

v$_o$

v''

v'''

u$_o$

u

u'

u''

u'''

Binding Energy (eV)
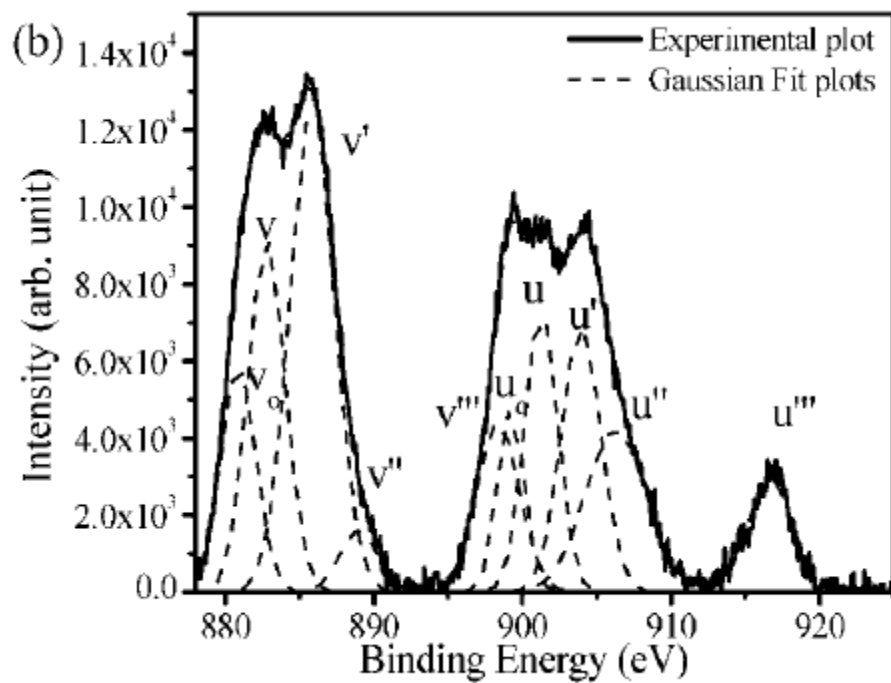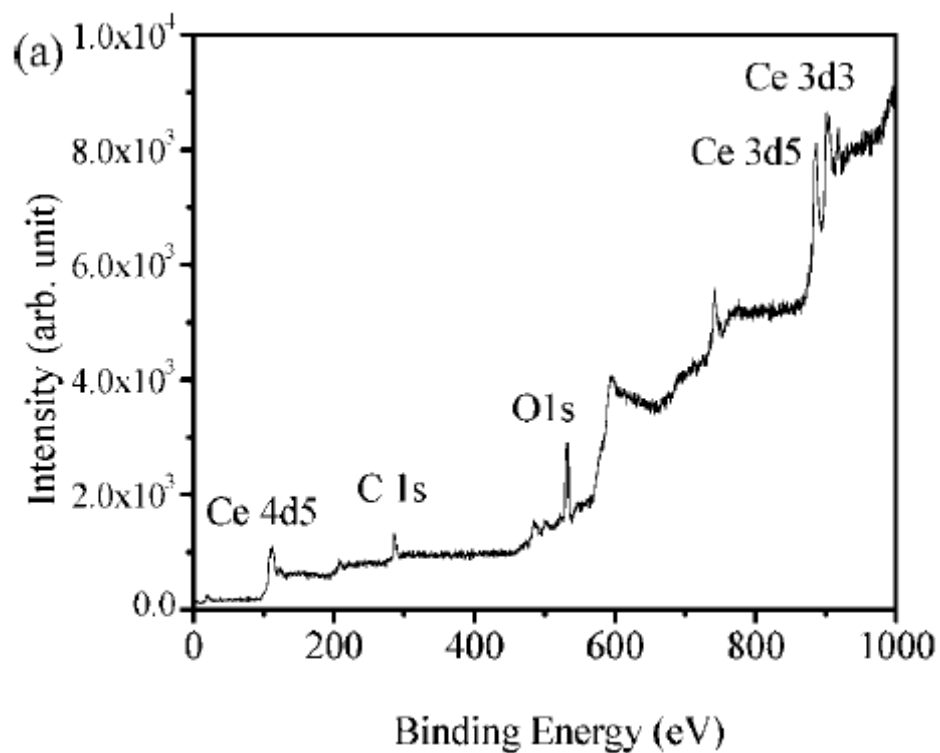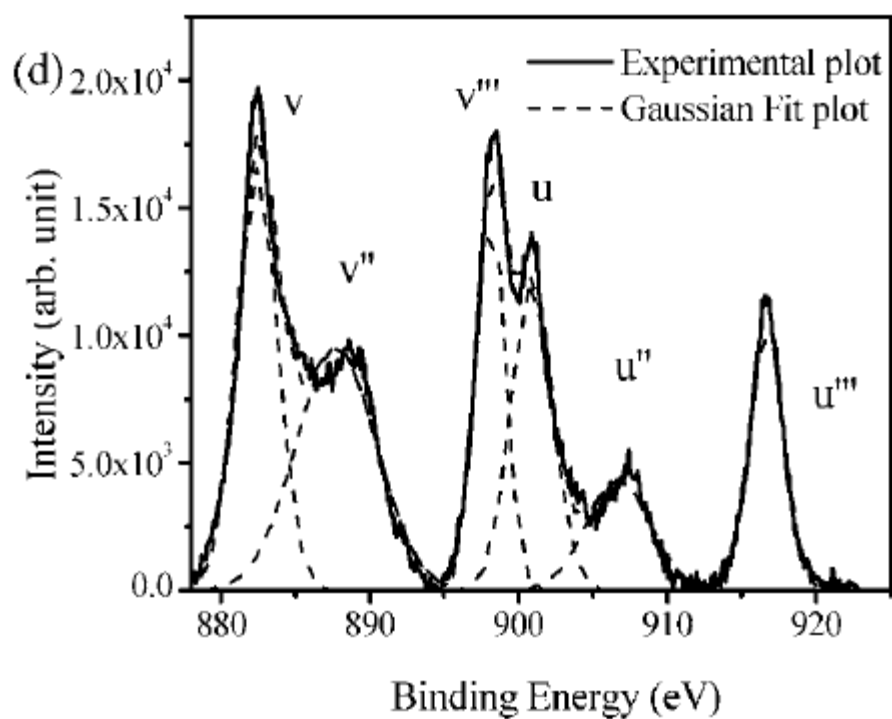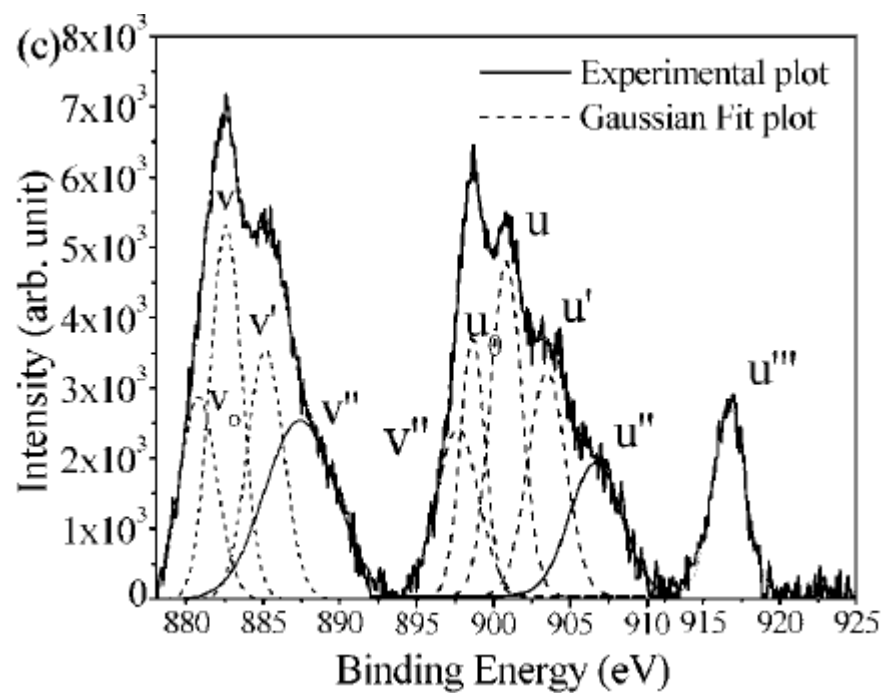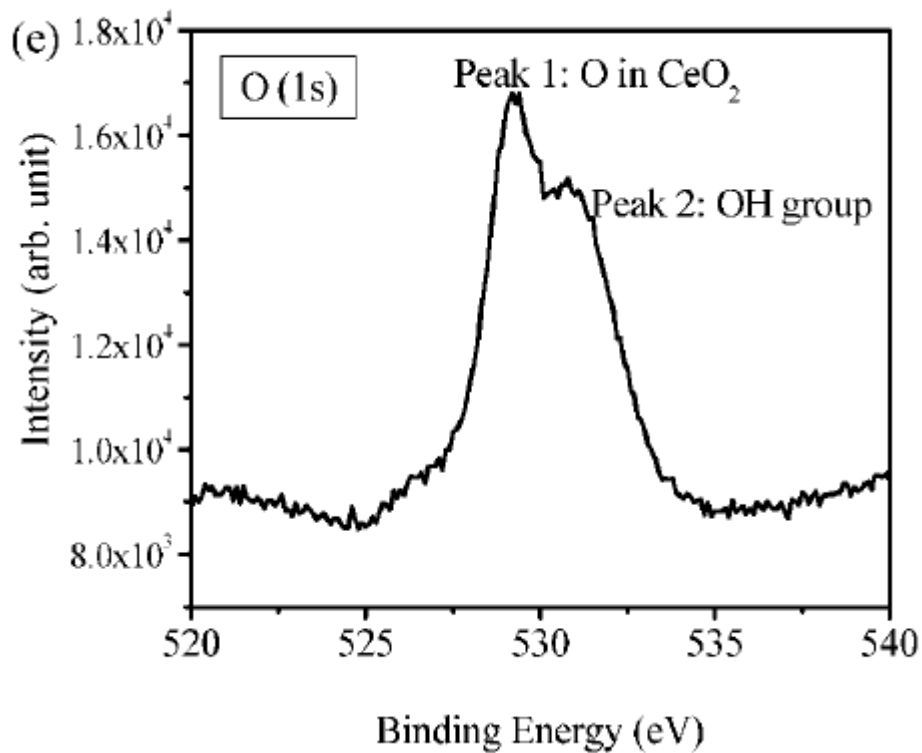
Figure 13 XPS spectra of the ceria NPs: (a) survey scan of the sample synthesized at room-temperature, (b, c and d) high-resolution plot along with the corresponding Gaussian fitting plots showing different valence states for Ce. (e) high resolution XPS spectrum in the region 520-540 cm^{-1} showing the details of O1s peak.

Table 2 XPS binding energies of individual peaks of the Ce (3d) spectrum for different

ceria NPs

	Ce $3d_{5/2}$					Ce $3d_{3/2}$				
	v_o	v	v′	V″	v‴	u_o	u	u′	u″	U‴
S2	880.68	882.87	885.88	888.56	898.25	899.16	901.1	903.89	906.44	916.81
S3	880.78	882.58	885.14	888.11	898.63	898.97	900.91	903.47	906.65	916.65
S4	-	882.45	-	887.75	898.1	-	900.88	-	906.67	916.67

CeO_2 crystallizes in the fluorite (CaF_2) structure, in which Ce^{4+} cation is surrounded by eight equivalent O^{2-} ions forming the corner of a cube, with each O^{2-} coordinated to four Ce^{4+} as shown schematically in Figure 14. Binary oxide semiconductors are always prone to anion vacancy. Our strong EN mediated synthesis helps to form oxygen deficit samples at RT where as high temperature helps to subsidize some of these oxygen vacancies. Due to the oxygen vacancy, the coordination number of Ce^{4+} to O^{2-} reduces from eight to seven and introduces Ce^{3+} ions into the crystal lattice, as shown in the scheme. Thus despite of having appreciable number of Ce^{3+} ions in the crystal, the NPs maintain their fluorite (CaF_2) structure.
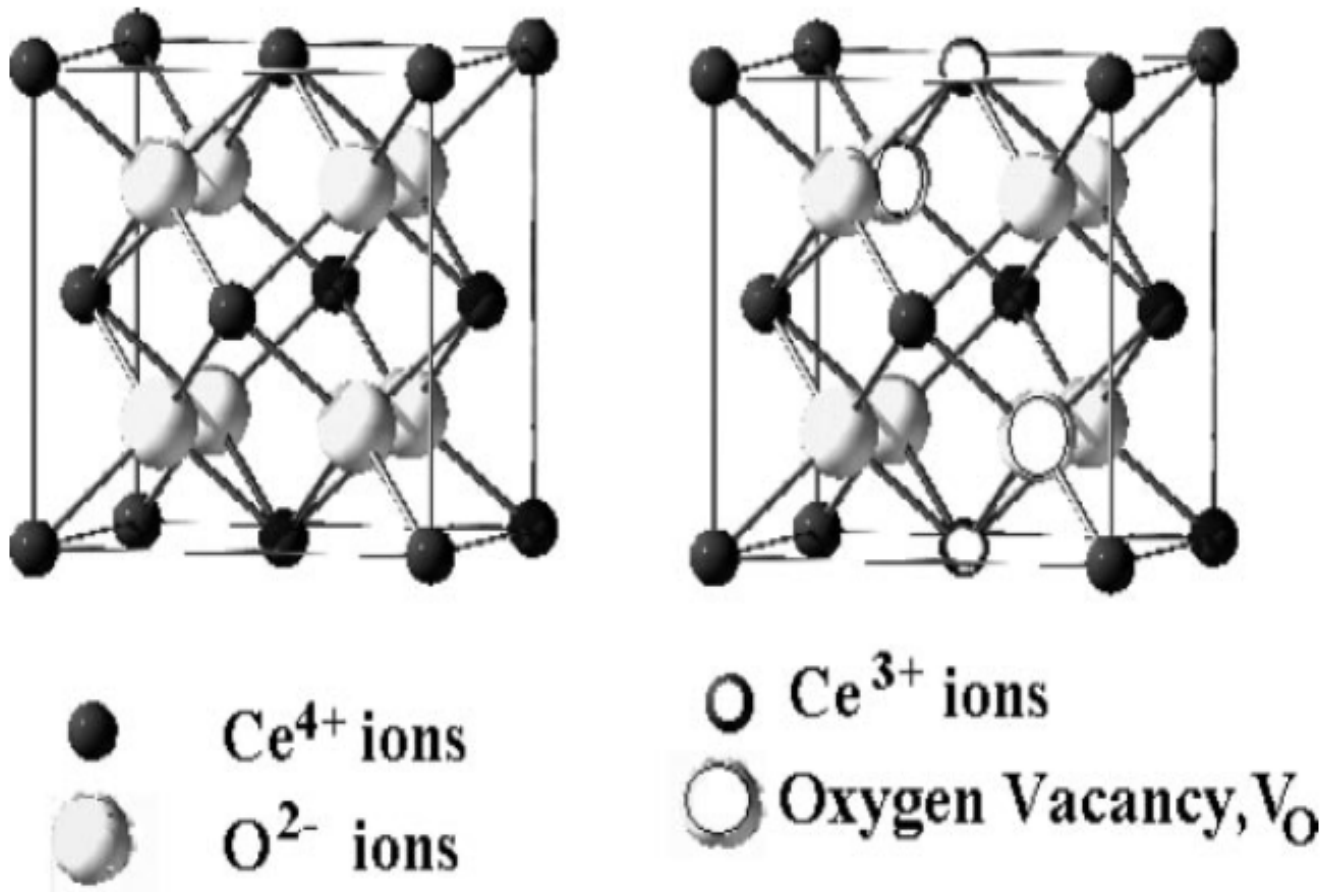
Figure 14 Schematic diagram of the fluorite (CaF2) crystal structure of ceria. Cartoon in the left shows perfect coordination between Ce4+ and neighboring O2- . The right cartoon shows the formation of Ce3+ due to the presence of oxygen vacancy.

3.2.1 Role of EN as Capping Agent

EN might have played a dual role in the formation of ultra fine ceria NPs. First, being a basic solution, it triggers controlled oxidation of the cerium nitrate salt to ceria. In addition it acts as a capping material providing mono-dispersed ultra-fine NPs at RT. The first role of EN acting as a basic catalyst to produce ceria from the cerium nitrate salt is demonstrated by the following reaction.

$$Ce(NO_3)_3 \cdot 6H_2O \xrightarrow{ethylenedia\min e} Ce(OH)_3 \rightarrow CeO_2 \qquad\qquad (1)$$
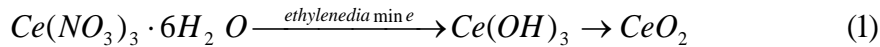
As the nascent ceria nucleation and growth starts, the EN molecules might attach on the cationic part of the surface atoms through its lone pair of electrons. Being a bi-dentate ligand (a pair of lone pair electrons associated with each molecule) EN could easily form complex with bivalent (group II) metal ions [43-49]. Since the ionic state of Cerium ion in the starting material is +3, this might prevent EN molecules to form a chelating complex (XRD, IR and SAED studies proved that the product was not a complex material but pure ceria), instead it behaved as a capping agent covering the surface of the nanocrystals. The EN layer surrounding the nanocrystals surface might prevent further inward diffusion of the constituent elements preventing the grain growth. These loosely bound EN molecules might have been exchanged by the hydroxyl ions during the process. As it can be seen that the Ce^{3+} oxidation state was converted to the Ce^{4+} at RT without any additional oxygen re-enforcement, the ceria NPs are expected to be rich in oxygen vacancy. This is already proved by the appearance of the Ce^{3+} oxidation state in the XPS spectrum of the CeO_2 crystals.

The presence of the mixed valence state indicated that these ultra fine nanocrystals might have antioxidant property and could used multiple times if it express auto generative recycle process. To demonstrate the auto-catalytic property of the ceria NPs, we carried out a UV–visible transmission spectroscopic study in absence and presence of hydrogen peroxide. The transmittance spectrum of the ceria NPs was recorded by dispersing the ceria NPs in de-ionized water (Figure 15a). In the next step, 10 µl H_2O_2 was added to the above solution, stirred for 1 min and the transmission spectrum was recorded again showing a large red shift compared to the previous spectra of the un-treated ceria NPs. This red-shift in the transmittance spectrum is attributed to the change in the oxidation state from Ce^{3+} to Ce^{4+}. The experimental solution treated with H_2O_2 was then preserved in the dark for further UV–visible measurements for the next 10 consecutive days. A gradual blue shift in the spectra was observed over time. This gradual blue shift (higher energy) reflects the regeneration (Ce^{4+}-Ce^{3+}) of the ceria NPs.

At the end of the 10 days, an additional H_2O_2 dose was administered to the solution and the corresponding UV–visible spectrum again exhibited red shift. The red shift of the UV visible spectrum (towards lower energy state) on exposure to H_2O_2 followed by a time dependent recovery toward a higher energy state (subsequent blue shift) indicated towards an auto-generated catalytic oxidative recovery (Ce^{3+}-Ce^{4+}-Ce^{3+}) cycle. These spectral changes were also associated with visible color change of the ceria NP solution (Figure 15b). Administration of the H_2O_2 induced a change in color from light yellow to dark-reddish brown which faded away with time. The color again turned dark after the second dose of H_2O_2 introduced at the 10th day of the experiment. These color changes are also characteristic of the valence state change of ceria NPs.
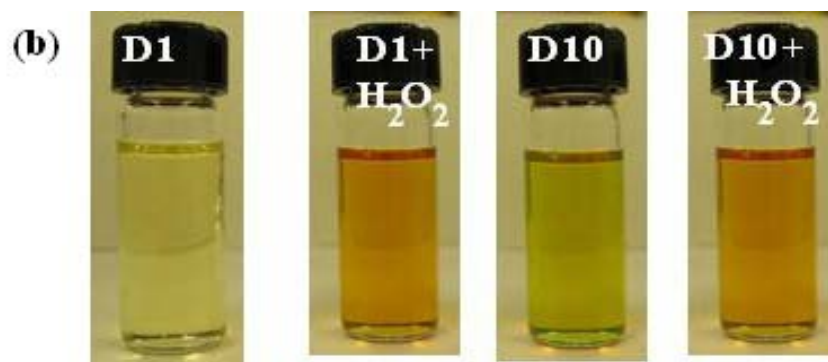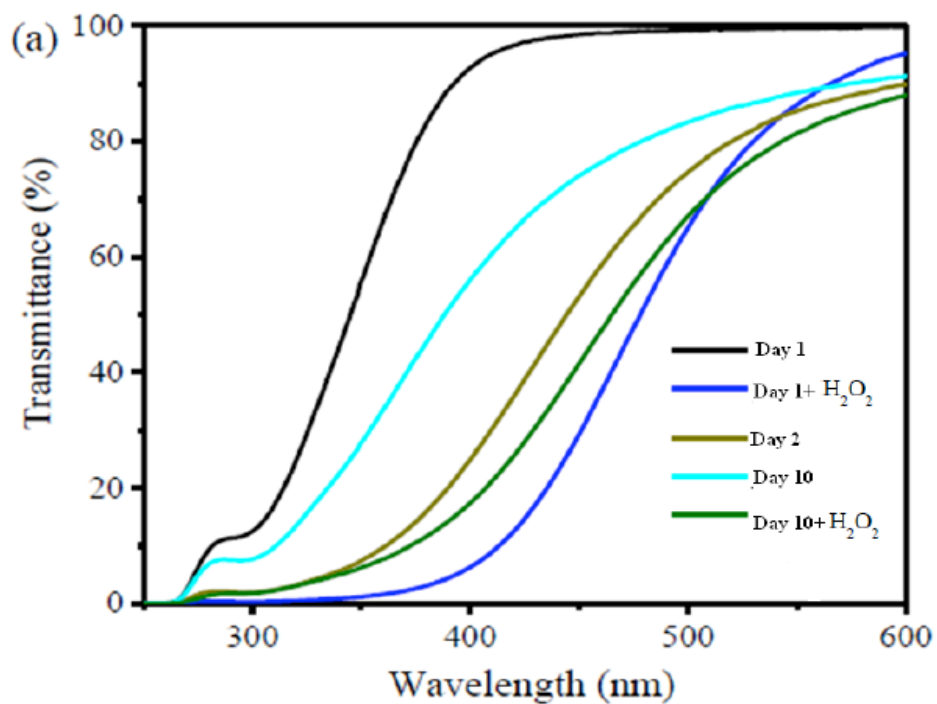
Figure 15 (a) UV-visible transmittance plots showing the autocatalytic behavior of the ceria NPs. (b) The digital image of the aqueous solution of the ceria NPs in absence and presence of hydrogen peroxide reflecting the valence state

CHAPTER 4: CONCLUSIONS

In this thesis work, two room temperature synthesis methods, dilute NaOH assisted and EN assisted, for producing high quality (ultra-small, monodispersed, crystalline and mixed Ce^{3+} and Ce^{4+} valence state), water-dispersible ceria NPs have been described. These methods are simple (one-pot synthesis), reproducible, cost-effective and can be optimized for large scale production. Ceria NPs were systematically characterized using different microscopic and spectroscopic material characterization techniques such as HRTEM, SAED, XPS, XRD, FT-IR, DLS and UV-Vis. TEM analysis confirmed the particle size of (3±0.5 nm) for NaOH assisted RT synthesis and (2.5 ± 0.2 nm) for EN assisted chemical route at RT. Studies reveal the formation of single crystalline ceria NPs with mixed valence state of Ce ions (Ce^{3+} and Ce^{4+}). The NPs exhibited autocatalytic behavior as investigated through a H_2O_2 test coupled with UV-visible transmission measurements. The role of EN as capping agent for the synthesis of ceria NPs was established by supporting solvothermal experiments. These studies indicated that the present ceria NPs could be directly used as an anti-oxidant in various biomedical applications.

REFERENCES

1.   Feynman, R., "There's Plenty of room at the bottom," *Engineering and Science* **1960,** 23, 22-36.

2.   Taniguchi, N. In *On the Basic Concepts of 'Nanotechnology'*, Proc. Intl Conf. Prod .Eng. Tokyo, Part II ,Japan Society of Precision Engineering, 1974; 1974.

3.   Drexler, K. E., *Engines of Creation*. Anchor Press: New York, 1986.

4.   Kratschmer, W., Lamb, L. D., Fostiropoulos, K., Huffman, D. R., Solid C-60 - A New Form of Carbon. *Nature* **1990,** 347, (6291), 354-358.

5.   Edwards, S., *The nanotech pioneers : where are they taking us?* . Weinheim : Wiley-VCH: 2006.

6.   Wautelet, M., Phase stability of electronically excited Si nanoparticles. *Journal of Physics-Condensed Matter* **2004,** 16, (12), L163-L166.

7.   Wu, Z. Y.; Bao, Z. X.; Cao, L.; Liu, C. X.; Li, Q. S.; Xie, S. S.; Zou, B. S., Electrical properties and phase transition of $CoFe_2O_4$ nanocrystals under pressure. *Journal of Applied Physics* **2003,** 93, (12), 9983-9987.

8.   Wilson, M., Kannangara, K., Smith, G., Simmons, M., Raguse, B. , *Nanotechnology : basic science and emerging technologies*. Chapman & Hall/CRC: Boca Raton, 2002.

9.   Gasman, L., *Nanotechnology applications and markets* Artech House: Boston, 2006.

10.   Tallury, P.; Payton, K.; Santra, S., Silica-based multimodal/multifunctional nanoparticles for bioimaging and biosensing applications. *Nanomedicine* **2008,** 3, (4), 579-592.

11.   Das, M.; Patil, S.; Bhargava, N.; Kang, J. F.; Riedel, L. M.; Seal, S.; Hickman, J. J., Auto-catalytic ceria nanoparticles offer neuroprotection to adult rat spinal cord neurons. *Biomaterials* **2007,** 28, (10), 1918-1925.

12.   Kar, S.; Patel, C.; Santra, S., Direct Room Temperature Synthesis of Valence State Engineered Ultra-Small Ceria Nanoparticles: Investigation on the Role of Ethylenediamine as a Capping Agent. *Journal of Physical Chemistry C* **2009,** 113, (12), 4862-4867.

13.   Perez, J. M.; Asati, A.; Nath, S.; Kaittanis, C., Synthesis of biocompatible dextran-coated nanoceria with pH-dependent antioxidant properties. *Small* **2008,** 4, (5), 552-556.

14.   Silva, G. A., Nanomedicine - Seeing the benefits of ceria. *Nature Nanotechnology* **2006,** 1, (2), 92-94.

15.   Tarnuzzer, R. W.; Colon, J.; Patil, S.; Seal, S., Vacancy engineered ceria nanostructures for protection from radiation-induced cellular damage. *Nano Letters* **2005,** 5, (12), 2573-2577.

16.   Evans, C. H., *Biochemistry of Lanthanides*. Plenum Press: New York 1990.

17.   Land, P. L., Defect Equilibra For Extended Point-Defects, With Application to Nonstoichiometric Ceria. *Journal of Physics and Chemistry of Solids* **1973,** 34, (11), 1839-1845.

18.   Suzuki, K. T., Electrical conductivity and lattice defects in nanocrystalline Cerium oxide Thin films. *Journal of American Ceramic Society* **2001,** 84, 2007-2014.

19.   Davis, V. T.; Thompson, J. S., Measurement of the electron affinity of cerium. *Physical Review Letters* **2002,** 88, (7).

20.   Herman, G. S., Characterization of surface defects on epitaxial CeO2(001) films. *Surface Science* **1999,** 437, (1-2), 207-214.

21.   Conesa, J. C., Computer Modeling of Surfaces and Defects in Cerium Dioxide. *Surface Science* **1995,** 339, (3), 337-352.

22.   Babu, S.; Velez, A.; Wozniak, K.; Szydlowska, J.; Seal, S., Electron paramagnetic study on radical scavenging properties of ceria nanoparticles. *Chemical Physics Letters* **2007,** 442, (4-6), 405-408.

23.   Dutta, P.; Pal, S.; Seehra, M. S.; Shi, Y.; Eyring, E. M.; Ernst, R. D., Concentration of Ce3+ and oxygen vacancies in cerium oxide nanoparticles. *Chemistry of Materials* **2006,** 18, (21), 5144-5146.

24.   Eguchi, K.; Setoguchi, T.; Inoue, T.; Arai, H., Electrical-Properties of Ceria-Based Oxides and Their Application To Solid Oxide Fuel-Cells. *Solid State Ionics* **1992,** 52, (1-3), 165-172.

25.   Feng, X. D.; Sayle, D. C.; Wang, Z. L.; Paras, M. S.; Santora, B.; Sutorik, A. C.; Sayle, T. X. T.; Yang, Y.; Ding, Y.; Wang, X. D.; Her, Y. S., Converting ceria polyhedral nanoparticles into single-crystal nanospheres. *Science* **2006,** 312, (5779), 1504-1508.

26.   Fu, Q.; Saltsburg, H.; Flytzani-Stephanopoulos, M., Active nonmetallic Au and Pt species on ceria-based water-gas shift catalysts. *Science* **2003,** 301, (5635), 935-938.

27.   Hibino, T.; Hashimoto, A.; Inoue, T.; Tokuno, J.; Yoshida, S.; Sano, M., A low-operating-temperature solid oxide fuel cell in hydrocarbon-air mixtures. *Science* **2000,** 288, (5473), 2031-2033.

28.   Izu, N.; Shin, W.; Murayama, N., Fast response of resistive-type oxygen gas sensors based on nano-sized ceria powder. *Sensors and Actuators B-Chemical* **2003,** 93, (1-3), 449-453.

29.   Kaspar, J.; Fornasiero, P., Nanostructured materials for advanced automotive de-pollution catalysts. *Journal of Solid State Chemistry* **2003,** 171, (1-2), 19-29.

30.   Laberty-Robert, C.; Long, J. W.; Lucas, E. M.; Pettigrew, K. A.; Stroud, R. M.; Doescher, M. S.; Rolison, D. R., Sol-gel-derived ceria nanoarchitectures: Synthesis, characterization, and electrical properties. *Chemistry of Materials* **2006,** 18, (1), 50-58.

31.   Patil, S.; Kuiry, S. C.; Seal, S.; Vanfleet, R., Synthesis of nanocrystalline ceria particles for high temperature oxidation resistant coating. *Journal of Nanoparticle Research* **2002,** 4, (5), 433-438.

32.   Wang, Z. L.; Feng, X. D., Polyhedral shapes of CeO2 nanoparticies. *Journal of Physical Chemistry B* **2003,** 107, (49), 13563-13566.

33.   Zhang, F.; Wang, P.; Koberstein, J.; Khalid, S.; Chan, S. W., Cerium oxidation state in ceria nanoparticles studied with X-ray photoelectron spectroscopy and absorption near edge spectroscopy. *Surface Science* **2004,** 563, (1-3), 74-82.

34.   Chen, J. P.; Patil, S.; Seal, S.; McGinnis, J. F., Rare earth nanoparticles prevent retinal degeneration induced by intracellular peroxides. *Nature Nanotechnology* **2006,** 1, (2), 142-150.

35.   Madler, L.; Stark, W. J.; Pratsinis, S. E., Flame-made ceria nanoparticles. *Journal of Materials Research* **2002,** 17, (6), 1356-1362.

36.   Oh, H.; Kim, S., Synthesis of ceria nanoparticles by flame electrospray pyrolysis. *Journal of Aerosol Science* **2007,** 38, (12), 1185-1196.

37.   Deshpande, S.; Patil, S.; Kuchibhatla, S.; Seal, S., Size dependency variation in lattice parameter and valency states in nanocrystalline cerium oxide. *Applied Physics Letters* **2005,** 87, (13).

38.   Adschiri, T., Supercritical hydrothermal synthesis of organic-inorganic hybrid nanoparticles. *Chemistry Letters* **2007,** 36, 1188-1193.

39.   Inoue, M.; Kimura, M.; Inui, T., Transparent colloidal solution of 2 nm ceria particles. *Chemical Communications* **1999**, (11), 957-958.

40.   Masui, T.; Fujiwara, K.; Machida, K.; Adachi, G.; Sakata, T.; Mori, H., Characterization of Cerium(IV) oxide ultrafine particles prepared using reversed micelles. *Chemistry of Materials* **1997,** 9, (10), 2197-2204.

41.   Wang, H.; Zhu, J. J.; Zhu, J. M.; Liao, X. H.; Xu, S.; Ding, T.; Chen, H. Y., Preparation of nanocrystalline ceria particles by sonochemical and microwave assisted heating methods. *Physical Chemistry Chemical Physics* **2002,** 4, (15), 3794-3799.

42.   Yu, T. Y.; Joo, J.; Park, Y. I.; Hyeon, T., Large-scale nonhydrolytic sol-gel synthesis of uniform-sized ceria nanocrystals with spherical, wire, and tadpole shapes. *Angewandte Chemie-International Edition* **2005,** 44, (45), 7411-7414.

43.   Biswas, S.; Kar, S., Fabrication of ZnS nanoparticles and nanorods with cubic and hexagonal crystal structures: a simple solvothermal approach. *Nanotechnology* **2008,** 19, (4).

44.   Datta, A.; Kar, S.; Ghatak, J.; Chaudhuri, S., Solvothermal synthesis of CdS nanorods: Role of basic experimental parameters. *Journal of Nanoscience and Nanotechnology* **2007,** 7, (2), 677-688.

45.   Dev, A.; Kar, S.; Chakrabarti, S.; Chaudhuri, S., Optical and field emission properties of ZnO nanorod arrays synthesized on zinc foils by the solvothermal route. *Nanotechnology* **2006,** 17, (5), 1533-1540.

46.   Kar, S.; Biswas, S., White light emission from surface-oxidized manganese-doped ZnS nanorods. *Journal of Physical Chemistry C* **2008,** 112, (30), 11144-11149.

47.   Kar, S.; Biswas, S.; Chaudhuri, S., Optical and magnetic properties of Mn-incorporated ZnS nanorods. *Synthesis and Reactivity in Inorganic Metal-Organic and Nano-Metal Chemistry* **2006,** 36, (2), 193-196.

48.   Kar, S.; Chaudhuri, S., Cadmium sulfide one-dimensional nanostructures: Synthesis, characterization and application. *Synthesis and Reactivity in Inorganic Metal-Organic and Nano-Metal Chemistry* **2006,** 36, (3), 289-312.

49.   Kar, S.; Santra, S.; Heinrich, H., Fabrication of high aspect ratio core-shell CdS-Mn/ZnS nanowires by a two step solvothermal process. *Journal of Physical Chemistry C* **2008,** 112, (11), 4036-4041.